Annals of Physics 412 (2020) 168000

Contents lists available at ScienceDirect

Annals of Physics

journal homepage: www.elsevier.com/locate/aop

Triphoton correlations in six-wave mixing

Siqiang Zhang [a,1], Wei Li [a,1], Kangkang Li [a], Yameng Li [a], Fan Mu [a], Yuan Feng [a], Yang Liu [b], Yanpeng Zhang [a,*]

[a] Key Laboratory for Physical Electronics and Devices of the Ministry of Education & Shaanxi Key Lab of Information Photonic Technique, Xi'an Jiaotong University, Xi'an 710049, China
[b] Key Laboratory of Transient Optics and Photonics, Xi'an Institute of Optics and Precision Mechanics, Chinese Academy of Sciences, Xi'an 710119, China

ARTICLE INFO

Article history:
Received 23 January 2019
Accepted 15 October 2019
Available online 2 November 2019

ABSTRACT

The generation of nonclassical multiphoton has aroused and renewed interest in recent years. Here, we theoretically propose a new method to generate a temporal triplet correlation via a spontaneous six-wave mixing process. In the dressed-state picture at atomic ensemble, we forecast two or more different resonant dispersion modes of each generated photons. With energy conservation condition, these resonant dispersion modes compose multiple six-wave mixing processes, and the different processes could beat with each other. When we only consider the nonlinear optical response, the coincidence counts of triplets perform as a damped Rabi oscillation (three conditional two-photon correlations with four or six periods) because of the destructive interference among the possible six-wave mixing processes. The coherent time in the system is determined by the effective dephasing rate. Furthermore, we study the triphoton correlation with the fifth-order nonlinear susceptibility and the phase matchings mixing.

1. Introduction

In the last decades, quantum mechanics has made great progress in science, but many mysteries remain unsolved. In this regard, the nonclasscial multiphoton provides a powerful tool to probe

* Corresponding author.
E-mail address: ypzhang@mail.xjtu.edu.cn (Y. Zhang).
[1] These authors contributed equally to this work.

https://doi.org/10.1016/j.aop.2019.168000
0003-4916/

the foundations of quantum theory and can be applied in quantum computing [1], quantum communication [2], quantum imaging technology [3] and many other fields. It is known that the most common method to generate entangled photon pairs is the spontaneous parametric down-conversion (SPDC) [4]. Some scientists have obtained photon triplets by using the cascaded SPDC process [5,6]. Since the SPDC process occurs in a nonlinear crystal and satisfies the phase-matching condition, the bandwidth of the generated photon pairs reaches several THz, and the coherent time is very short. In contrast, with the SPDC, the correlated photons generated from the atomic ensemble via a spontaneous parametric multiple-wave mixing process have many advantages, such as the narrow bandwidth, long coherent time, and high conversion efficiency. Many attempts have been made in the last ten years. The Harris group [7,8] obtained entangled photon pairs by using the electromagnetically induced transparency (EIT) [9] and spontaneous parametric four-wave mixing process. Wen [10] theoretically obtained photon triplets via two cascaded four-wave mixing processes. Many useful methods have been reported in both theoretical [11–19] and experimental studies [20–22]. In addition, some researchers combined a spontaneous Raman scattering process in a hot Rb atomic cell with an SPDC process and realized the hybrid-cascaded photon triplets [23]. Despite such rapid progress, no methods that demonstrate the generation of photon triplets in one single physical progress have been reported.

In this paper, we propose a new method to create photon triplets via a single six-wave mixing process in an atomic ensemble. Since we only use one spontaneous six-wave mixing (SSWM) process with no secondary step (like in the cascaded methods), the photon triplets should have a higher emission efficiency without post selection and long coherence. Furthermore, since the nonlinear susceptibility of the optical response plays a dominant role in determining the wave packet of the photon triplets and destructive interference among multiple modes of the spontaneous six-wave mixing processes, the coincidence counts of triplets perform as a damped Rabi oscillation. The outcome has a wide range of application prospects.

The paper is organized as follows. In Section 2, we calculate the triphoton wave function and derive the third-order intensity correlation function. In Section 3, we discuss the optical responses, which contain two situations: nonlinear response and linear response. In Section 4, we show the mechanism of triphoton generation via the nonlinear response and explain the frequency modes of the generated fields in the presence of the dressing field. In Section 5, we show the numerical simulation picture. In Section 6, we summarize the methods and present the outlook.

2. Schematic of the triphoton state function

The schematic of triphoton generation via a four-level "tri-Λ" atomic system is shown in Fig. 1(b). The relevant energy levels are $5S_{1/2}$, F = 2 ($|1\rangle$), $5S_{1/2}$, F = 3 ($|2\rangle$), $5P_{1/2}$ ($|3\rangle$) and $5P_{3/2}$ ($|4\rangle$). A simplified experimental setup of this process is illustrated in Fig. 1(a). In this setup, the SSWM process occurs based on a medium of atomic vapor. With identical four-level atoms initially prepared in their ground level $|1\rangle$, the medium is confined in a long, thin cylindrical volume with length L. In Fig. 1(a), a weak pump beam $\boldsymbol{E}_1$ (frequency ω_1, wave vector $\boldsymbol{k}_1$, Rabi frequency G_1, wavelength 795 nm) is applied to the atomic transition $|1\rangle \rightarrow |3\rangle$ with a detuning Δ_1. $\Delta_i = \Omega_i - \omega_i$ is the detuning, which is defined as the difference between the resonant transition frequency Ω_i and laser frequency ω_i of $\boldsymbol{E}_i$. A strong coupling beam $\boldsymbol{E}_2$ (ω_2, $\boldsymbol{k}_2$, G_2, 780 nm) at the near-resonant frequency of the atomic transition $|2\rangle \rightarrow |4\rangle$ with detuning Δ_2 is introduced and counterpropagates with $\boldsymbol{E}_1$. Another coupling beam $\boldsymbol{E}_3$ (ω_3, $\boldsymbol{k}_3$, G_3, 780 nm) propagates in the $\boldsymbol{E}_2$ direction and is applied to the atomic transition $|1\rangle \rightarrow |4\rangle$ with detuning Δ_3. All beams are coupled to the center of the medium by optical lenses. Then, with the phase-matching condition $\boldsymbol{k}_1 + \boldsymbol{k}_2 + \boldsymbol{k}_3 = \boldsymbol{k}_{S1} + \boldsymbol{k}_{S2} + \boldsymbol{k}_{S3}$ and low-gain limit, the SSWM process will spontaneously occur, which can generate the correlated triphoton $\boldsymbol{E}_{S1}$, $\boldsymbol{E}_{S2}$ and $\boldsymbol{E}_{S3}$ satisfying the energy conservation: $\omega_1 + \omega_2 + \omega_3 = \omega_{s1} + \omega_{s2} + \omega_{s3}(\varpi_{s1} + \delta_1 + \varpi_{s2} + \delta_2 + \varpi_{s3} + \delta_3)$, as illustrated in Fig. 1(c). Here, the pump beam has a much smaller power than the coupling beams. Meanwhile, the pump beam is used at far off resonance with a large detuning. Thus, the quantum atomic noise can be suppressed, and the atomic population is primarily maintained at the ground state. In addition, the strong coupling beams $\boldsymbol{E}_2$ and $\boldsymbol{E}_3$ with near-resonance contribute to form a Λ electromagnetically induced

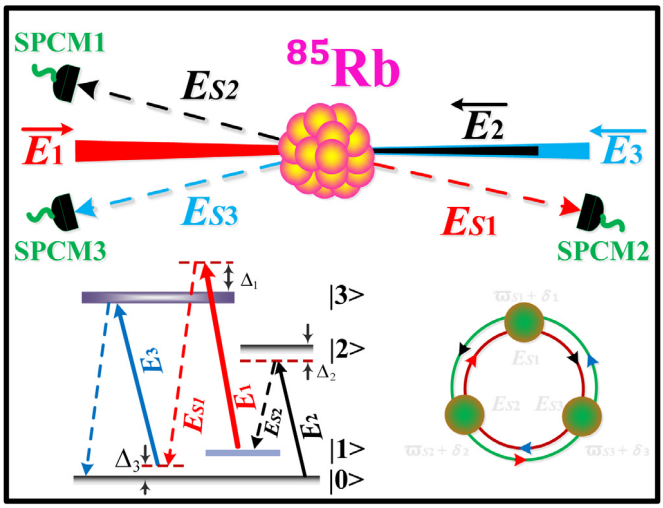

Fig. 1. (a) Spatial beams alignment of the generation triphoton in six-wave mixing; The generated photons are detected by three single-photon counting modules (SPCM1–SPCM3) based on the avalanche photodiodes, and the distances between the SPCMs and the center of the medium are uniform. (b) Mechanisms of the triphoton generation from a four-level configuration. In the presence of pump ω_1 and two coupling beams ω_2 and ω_3, triphotons ω_{S1}, ω_{S2} and ω_{S3} are spontaneously generated from the SSWM process in the low-gain regime. (c) Energy conservation of the multimode triphoton.

transparency (EIT) scheme. Therefore, the coupling beams can assist the SSWM nonlinear process and create a transparency window for photons $\boldsymbol{E}_{S2}$ and $\boldsymbol{E}_{S3}$ with slow-light effect. The generated triphoton can be detected by three single-photon counting modules (SPCM). Moreover, because our theory is based on the cool atomic ensemble, we do not consider the Doppler broadening, polarization effects and quantum Langevin noise. We focus on the triphoton temporal correlation and the interference of the multimode SSWM. Most biphotons generated from the four-wave mixing processes are eliminated from the counting regime by placing the detectors at appropriate angles using filters and Fabry–Perot cavities. However, some biphotons and uncorrelated single photons remain, which constitute the background of the coincidence count of triphoton.

In the interaction picture, the effective interaction Hamiltonian for the six-wave mixing process can be written as (we ignore the reflections from the system surfaces and use the rotating-wave approximation):

$$H_I = \varepsilon_0 \int_V d^3z \chi^{(5)} E_1^{(+)} E_2^{(+)} E_3^{(+)} E_{S3}^{(-)} E_{S2}^{(-)} E_{S1}^{(-)} + H.c. \tag{1}$$

where $\chi^{(5)}$ is the fifth-order nonlinear susceptibility to the generated photon field defined by the nonlinear polarization; V is the interaction volume illuminated by the input field together; $H.c$ is the Hermitian conjugate; $E_1^{(+)}$, $E_2^{(+)}$ and $E_3^{(+)}$ are the positive-frequency parts of the strong input classical fields, which are given as:

$$E_1^{(+)} = E_1 e^{i(k_1 z - \omega_1 t)}, E_2^{(+)} = E_2 e^{i(k_2 z - \omega_2 t)}, E_3^{(+)} = E_3 e^{i(k_3 z - \omega_3 t)}, \tag{2}$$

where k_i are the field wavenumbers; $E_i = i\sqrt{\hbar\omega_i / 2\varepsilon_0 n_i^2 V_q}$, V_q is the quantization volume; and $n_i = \sqrt{1 + \mathrm{Re}(\chi_{si})}$, which is the refractive index experienced by each weak field. The generated

photons are given by the quantized fields,

$$E_{S1}^{(+)}(z,t) = \frac{1}{\sqrt{2\pi}} \int d\omega \sqrt{\frac{2\hbar\varpi_{S1}}{c\varepsilon_0 A}} \hat{a}_{S1}(\omega)\, e^{i[\hat{k}_{S1}\cdot\hat{z}-\omega t]}, \tag{3a}$$

$$E_{S2}^{(+)}(z,t) = \frac{1}{\sqrt{2\pi}} \int d\omega \sqrt{\frac{2\hbar\varpi_{S2}}{c\varepsilon_0 A}} \hat{a}_{S2}(\omega)\, e^{-i[\hat{k}_{S2}\cdot\hat{z}+\omega t]}, \tag{3b}$$

$$E_{S3}^{(+)}(z,t) = \frac{1}{\sqrt{2\pi}} \int d\omega \sqrt{\frac{2\hbar\varpi_{S3}}{c\varepsilon_0 A}} \hat{a}_{S3}(\omega)\, e^{i[\hat{k}_{S3}\cdot\hat{z}-\omega t]}, \tag{3c}$$

where A is the single-mode cross-section area. $\hat{a}_{S1}$, $\hat{a}_{S2}$ and $\hat{a}_{S3}$ are the photon annihilation operators of output modes $\boldsymbol{S}_1$, $\boldsymbol{S}_2$ and $\boldsymbol{S}_3$, respectively; c is the speed of light in vacuum; ε_0 is the vacuum permittivity; and ϖ_i is the central frequency of the generated photons. Substituting the electric fields in Eqs. (2) and (3) into Eq. (1) gives:

$$\hat{H}_I = W_1 \int d\omega_{S1} d\omega_{S2} d\omega_{S3} \kappa \, \mathrm{sinc}\left(\frac{\Delta kL}{2}\right) \hat{a}_{S1}^{\dagger} \hat{a}_{S2}^{\dagger} \hat{a}_{S3}^{\dagger} e^{-i\Delta\omega t} + H.c. \tag{4}$$

where $\kappa = -i\sqrt{\varpi_{S1}\varpi_{S2}\varpi_{S3}/c^3}\,\chi^{(5)}(\omega_{S1},\omega_{S2},\omega_{S3})E_1E_2E_3$ is the nonlinear parametric coupling coefficient; $W_1 = i\sqrt{\hbar^3/\pi^3\varepsilon_0^3 A^3}$ is a constant; $\Delta\omega = \omega_1 + \omega_2 + \omega_3 - \omega_{S1} - \omega_{S2} - \omega_{S3}$; $\Delta k = k_{S1} + k_{S2} + k_{S3} - k_1 - k_2 - k_3$ is the phase mismatching along the z axis. When $\Delta k = 0$, the phase-matching condition perfectly holds.

According to the first-order perturbation in the interaction picture, the photon state at the output surface is approximately a linear superposition of $|0\rangle$ and $|\Psi\rangle$, where $|0\rangle$ is the vacuum state. Since the vacuum is not detectable, we may ignore it. The photon triplets state $|\Psi\rangle$ can be expressed as:

$$|\psi\rangle = \frac{-i}{\hbar} \int_{-\infty}^{+\infty} dt \hat{H}_I |0\rangle \tag{5}$$

Combining with Eqs. (4) and (5), $e^{-i\Delta\omega t}$ becomes $2\pi\delta(\Delta\omega)$, which indicates the energy conservation of the SSWM process and causes the frequency entanglement of the triphoton state. Eq. (5) can be rewritten as:

$$\begin{aligned} |\psi\rangle &= \int d\omega_{S1} d\omega_{S2} d\omega_{S3} \kappa \, \mathrm{sinc}\left(\frac{\Delta kL}{2}\right) \hat{a}_{S1}^{\dagger} \hat{a}_{S2}^{\dagger} \hat{a}_{S3}^{\dagger} \delta(\Delta\omega) |0\rangle \\ &= \int d\omega_{S1} d\omega_{S2} d\omega_{S3} \kappa(\omega_i) \, \mathrm{sinc}\left(\frac{\Delta kL}{2}\right) \hat{a}_{S1}^{\dagger} \hat{a}_{S2}^{\dagger} \hat{a}_{S3}^{\dagger} |0\rangle \end{aligned} \tag{6}$$

From Eq. (6), we can predict that the triphoton state is entangled in frequency and wavenumber. $\kappa(\omega_i) = \kappa(\omega_{S1}, \Delta\omega + \omega_{S2}, \omega_{S3})$ shows the entanglement in the frequency space, which is the result of the energy conservation condition. $\mathrm{Sinc}(\Delta kL/2)$ indicates the wavenumber entanglement because it cannot be factorized into three independent functions, which only contain k_{S1}, k_{S2} and k_{S3}, respectively.

To discuss the optical properties of the generated photons from a four-level system, we begin to consider the triphoton coincidence counting rate. We suppose that detectors SPCM1, 2 and 3 detect photons with frequencies ω_{S1}, ω_{S2} and ω_{S3}, respectively. Assuming perfect detection efficiency, the averaged triphoton coincidence counting rate is defined by

$$R_{cc} = \lim_{T\to\infty} \frac{1}{T} \int_0^T dt_{S1} \int_0^T dt_{S2} \int_0^T dt_{S3} G^{(3)} M_1(t_{S2} - t_{S1}) M_2(t_{S3} - t_{S1}), \tag{7}$$

where $M_1(t_{S1} - t_{S2})$ and $M_2(t_{S3} - t_{S2})$ are the coincidence window functions, and we consider $M_i = 1$ for $M_1(t_{S1} - t_{S2})\ |t_{S1} - t_{S2}| < t_{cc}$ and $M_2(t_{S3} - t_{S2})\ |t_{S3} - t_{S2}| < t_{cc}$; otherwise, $M_i = 0$. $G^{(3)}$ is the third-order intensity correlation function of the triphoton, which can be written as:

$$G^{(3)} = \left|\langle\Psi| E_{S1}^{(-)} E_{S2}^{(-)} E_{S3}^{(-)} E_{S3}^{(+)} E_{S2}^{(+)} E_{S1}^{(+)} |\psi\rangle\right| = \left|\langle 0| E_{S3}^{(+)} E_{S2}^{(+)} E_{S1}^{(+)} |\psi\rangle\right|^2 = |B(\tau_{S1}, \tau_{S2}, \tau_{S3})|^2, \tag{8}$$

where $\tau_{Si} = t_{Si} - r_{Si}/c$ and r_{Si} is the optical path of the ith photon from the output surface of the medium to the detector. For simplicity, we consider $r_{S1} = r_{S2} = r_{S3}$. $B(\tau_{s1}, \tau_{s2}, \tau_{s3})$ is called the triphoton amplitude. By using Eqs. (3) and (6), we obtain:

$$B(\tau_{S1}, \tau_{S2}, \tau_{S3}) = W_2 \int d\,\omega_{S1} d\,\omega_{S2} d\,\omega_{S3} \kappa\,(\omega_i)\,\Phi(\Delta kL) e^{-i(\omega_{S1}\tau_{S1}+\omega_{S2}\tau_{S2}+\omega_{S3}\tau_{S3})}, \tag{9}$$

where W_2 is a constant that absorbs all constants and slowly varying terms and $\Phi(\Delta kL) = \mathrm{Sin}\ c(\Delta kL/2) e^{iL(k_{S1}+k_{S2}+k_{S3})/2}$ is the longitudinal detuning function that determines the natural spectral width. From Eq. (9), the pattern of the triphoton amplitude is determined by both nonlinear parametric coupling coefficient k and longitudinal detuning function Φ.

3. Optical responses of the SSWM process

As presented in Eq. (9), the pattern of the triphoton amplitude is determined by both fifth-order nonlinear susceptibility and longitudinal detuning function. Therefore, in this section, we examine the linear and nonlinear optical responses to the generated fields.

3.1. Nonlinear optical responses

According to the theory of perturbation chain [24], the fifth-order nonlinear susceptibilities for the generated fields are

$$\chi_{S1}^{(5)} = \frac{N_0}{d_{30} d_{00} d_{20} d_{20} d'_{30}},\ \chi_{S2}^{(5)} = \frac{N_0}{d_{31} d_{01} d'_{31} d'_{01} d_{21}},\ \chi_{S3}^{(5)} = \frac{N_0}{d'_{20} d'_{10} d''_{30} d'_{00} d'''_{30}}, \tag{10}$$

where $N_0 = 2N\mu_{02}\mu_{13}\mu_{03}\mu_{21}\mu_{30}\mu_{30}/\varepsilon_0\hbar^5$ is the constant; μ_{ij} are the electric dipole matrix elements; $d_{30} = \Gamma_{30} + i\Delta_3$, $d_{00} = \Gamma_{00} + i\delta_3$, $d_{20} = \Gamma_{20} + i\delta_3 + i\Delta_2$, $d_{10} = \Gamma_{10} - i\delta_1$, $d'_{30} = \Gamma_{30} - i\delta_1 + i\Delta_1$, $d_{31} = \Gamma_{31} + i\Delta_1$, $d_{01} = -\Gamma_{01} + i\delta_1$, $d'_{31} = -\Gamma_{31} + i\delta_1 + i\Delta_3$, $d'_{01} = \Gamma_{01} + i\delta_1 + i\delta_3$, $d_{21} = \Gamma_{21} + i\delta_1 + i\delta_3 + i\Delta_2$, $d'_{20} = \Gamma_{20} + i\Delta_2$, $d'_{10} = \Gamma_{10} - i\delta_1 - i\delta_3$, $d''_{30} = \Gamma_{30} - i\delta_1 - i\delta_3 + i\Delta_1$, $d'_{00} = \Gamma_{00} - i\delta_3$, and $d'''_{30} = \Gamma_{30} - i\delta_3 + i\Delta_3$; Γ_{ij} is the dephasing rate of coherence $|j\rangle \to |i\rangle$, $\Delta_i = \Omega_i - \omega_i$ is the detuning, which is defined as the difference between resonant transition frequency Ω_i and laser frequency ω_i of $\boldsymbol{E}_i$.

3.2. Linear optical responses

The linear susceptibilities of the generated photons are

$$\chi_{s1} = \frac{N_1\mu_{14}^2}{\dot{d}_{41}},\ \chi_{s2} = \frac{N_1\mu_{23}^2}{\dot{d}_{23}},\ \chi_{s3} = \frac{N_1\mu_{14}^2}{\ddot{d}_{41}}, \tag{11}$$

where $N_1 = 2N/\varepsilon_0\hbar$ is the constant, $\dot{d}_{30} = \Gamma_{30} + i(\Delta_1 - \delta_1)$, $\dot{d}_{12} = \Gamma_{12} + i(\Delta_2 - \delta_2)$, and $\ddot{d}_{30} = \Gamma_{30} + i(\Delta_3 + \delta_1 + \delta_2)$. The complex wavenumbers of the generated photons are obtained from the relations $k_{si} = (\varpi_{si} + \delta_i)/v_{si}$ and $v_{si} = c/[n_i + \omega_{si}(dn_i/d\,\omega_{si})]$, which are the group velocities of generated photons through the medium. From the above description, we obtain

$$v_{S1} = \frac{c}{1 + \frac{\omega_{31}}{2}\frac{d(\mathrm{Re}[\chi_{S1}(\omega)])}{d\,\omega}} = \frac{c\left(\Gamma_{03}^2 + \Delta_1^2\right)^2}{\left(\Gamma_{03}^2 + \Delta_1^2\right)^2 - \omega_{31}N_1\mu_{03}^2\Gamma_{03}}, \tag{12a}$$

$$v_{S2} = \frac{c}{1 + \frac{\omega_{41}}{2}\frac{d(\mathrm{Re}[\chi_{S2}(\omega)])}{d\,\omega}} = \frac{c\left(\Gamma_{12}^2 + \Delta_2^2\right)^2}{\left(\Gamma_{12}^2 + \Delta_2^2\right)^2 - \omega_{41}N_1\mu_{02}^2\Gamma_{12}}, \tag{12b}$$

$$v_{S3} = \frac{c}{1 + \frac{\omega_{41}}{2}\frac{d(\mathrm{Re}[\chi_{S3}(\omega)])}{d\,\omega}} = \frac{c\left(\Gamma_{03}^2 + \Delta_3^2\right)^2}{\left(\Gamma_{03}^2 + \Delta_3^2\right)^2 - \omega_{03}N_1\mu_{03}^2\Gamma_{03}}. \tag{12c}$$

Since Δ_1 is a large detuning, $\left(\Gamma_{03}^2+\Delta_1^2\right)^2 \gg N_1\mu_{03}^2\Gamma_{03}$. The group velocity of $\boldsymbol{E}_{S1}$ is approximately equal to c. Therefore, the wavenumber mismatch can be written as

$$\Delta k = k_{S1}+k_{S2}+k_{S3}-k_1-k_2-k_3 = (\frac{1}{v_{S2}}-\frac{1}{v_{S3}})\delta_2-\frac{1}{v_{S3}}\delta_1, \tag{13}$$

The bandwidth resulting from the group delay can be estimated as $\Delta\omega_{gi}\sim v_{Si}/L$. We consider two cases here: (a) $v_{S2}>v_{S3}$ and (b) $v_{S2}<v_{S3}$. In case (a), $\Delta\omega_{g2}>\Delta\omega_{g3}$. In case (b), $\Delta\omega_{g2}<\Delta\omega_{g3}$. These two cases are equivalent in principle, so we only consider case (a) and write $\Delta\omega_{g2}$ as $\Delta\omega_g$. According to the relationship $T(\omega)=e^{-\mathrm{Im}(\chi_{si})kL}(i=1,3)$, we know that the transmission spectral widths limit the propagations of the generated fields, whereas the imaginary part of the linear susceptibility determines this transmission spectral width. Therefore, the transmission profile serves as the control field, which controls the transmission of the $\boldsymbol{E}_{S2}$ and $\boldsymbol{E}_{S3}$ photons.

The wave function of the triphoton is generally a convolution of nonlinear and linear optical responses, and the properties of the triphoton amplitude can be determined by either response. In our paper, with the strong dressing field, the effective coupling Rabi frequency Ω_e and linewidth γ_e from the nonlinear optical response are smaller than the phase-matching bandwidth $\Delta\omega_g$ of the linear optical response. In addition, the group speed of fast light is close to the speed of light with a strong dressing effect. In this case, we can calculate the phase-matching $\Delta k\approx 0$. Thus, the longitudinal detuning function $\Phi\ (\Delta kL)$ that represents the linear optical response can be approximated as 1; considering the nonlinear susceptibility, it plays a major role in determining the spectral width. For another case, with the weak dressing field, the nonlinear susceptibility can be approximated as constant. Meanwhile, Ω_e and γ_e are larger than $\Delta\omega_g$, the group speeds of photons are slower than the speed of light, so $\Delta k\neq 0$, and linear susceptibility plays a major role in determining the spectral width. In this paper, we mainly discuss the case of the strong dressing effect and focus on the nonlinear susceptibility. In this case, the coincidence counts of triplets perform as a damped Rabi oscillation.

4. Multi-mode SSWM process

In this section, we will discuss the effect of leading into the dressing field. By enhancing the power of $\boldsymbol{E}_1$, we introduce a dressing field.

$$\chi_{S1}^{(5)} = \frac{N_0}{d_{30}d_{00}^{d}d_{20}d_{10}d_{30}'} = \frac{N_0}{(\Gamma_{30}+\mathrm{i}\Delta_3)P_1(\delta_1,\delta_3)}, \tag{14}$$

$$\chi_{S2}^{(5)} = \frac{N_0}{d_{31}d_{01}d_{31}'d_{01}^{'d}d_{21}} = \frac{N_0}{(\Gamma_{31}+i\Delta_1)\,P_2(\delta_1,\delta_2)}, \tag{15}$$

$$\chi_{S3}^{(5)} = \frac{N_0}{d_{20}'d_{10}^{'d}d_{30}''d_{00}^{'d}d_{30}'''} = \frac{N_0}{\varepsilon_0\hbar\,(\Gamma_{20}+i\Delta_2)\,P_3(\delta_2,\delta_3)}, \tag{16}$$

where $P_1(\delta_1,\delta_3)=(\delta_3-\Delta_1/2-\Omega_{e1}/2+i\Gamma_{e1})(\delta_3-\Delta_1/2+\Omega_{e1}/2+i\Gamma_{e1})(\delta_3+\Delta_2+i\Gamma_{20})(\delta_1+i\Gamma_{10})(\delta_1-\Delta_1+i\Gamma_{30})$,

$$\begin{aligned}
P_2(\delta_1,\delta_2) &= (\delta_1+i\Gamma_{01})\,(\delta_1+\Delta_3+i\Gamma_{31})\,(\delta_2-\Delta_1/2-\Omega_{e2}/2+i\Gamma_{e2})\\
&\quad\times\,(\delta_2-\Delta_1/2+\Omega_{e2}/2+i\Gamma_{e2})\,(\delta_2-\Delta_2+i\Gamma_{21})\,,\\
P_3(\delta_2,\delta_3) &= (\delta_2-\Delta_1/2-\Omega_{e3}/2+i\Gamma_{e3})(\delta_2-\Delta_1/2+\Omega_{e3}/2+i\Gamma_{e3})\,(\delta_3-\Delta_3+i\Gamma_{30})\\
&\quad\times\,(\delta_2-i\Gamma_{10})\,(\delta_3+\Delta_1/2-\Omega_{e4}/2+i\Gamma_{e4})(\delta_3+\Delta_1/2+\Omega_{e4}/2+i\Gamma_{e4}),\\
d_{00}^{d} &= G_1^2/(\Gamma_{12}+i\delta_3-i\Delta_1), \qquad d_{01}^{'d} = G_1^2/(\Gamma_{42}+i\delta_1+i\delta_3-i\Delta_1),\\
d_{10}^{'d} &= G_1^2/(\Gamma_{41}-i\delta_1-i\delta_3-i\Delta_1), \qquad d_{00}^{'d} = G_1^2/(\Gamma_{22}-i\delta_3-i\Delta_1),\\
\Omega_{e1} &= (\Delta_1^2+4(G_1^2+\Gamma_{10}\Gamma_{00}))^{1/2}, \qquad \Gamma_{e1} = (\Gamma_{00}+\Gamma_{10})/2,
\end{aligned}$$

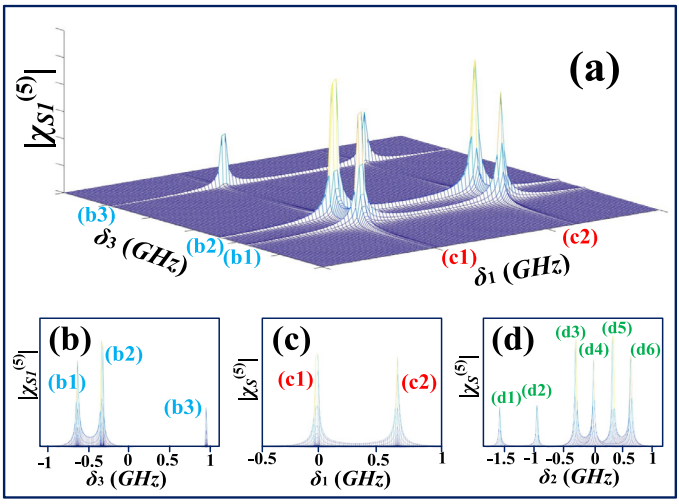

Fig. 2. (a) Resonances in the fifth-order nonlinear susceptibility $|\chi_{S1}{}^{(5)}|$ with dressing field $|G_1|^2$; (b) resonances in the dimension of δ_3; (c) resonances in the dimension of δ_1; (d) resonances in the dimension of δ_2.

$$\Omega_{e2} = (\Delta_1^2 + 4(G_1^2 + \Gamma_{10}\Gamma_{00}))^{1/2}, \qquad \Gamma_{e2} = (\Gamma_{11} + \Gamma_{10})/2,$$
$$\Omega_{e3} = (\Delta_1^2 + 4(G_1^2 + \Gamma_{10}\Gamma_{30}))^{1/2},$$

$\Gamma_{e3} = (\Gamma_{30} + \Gamma_{10})/2$, $\Omega_{e4} = (\Delta_1^2 + 4(G_1^2 + \Gamma_{11}\Gamma_{00}))^{1/2}$, and $\Gamma_{e4} = (\Gamma_{11} + \Gamma_{00})/2$. We obtain the specific value of δ by minimizing the denominator of $\chi^{(5)}$. Ω_{ei} represent the periods of Rabi oscillation; Γ_{ei} is the decay rate; and Γ_{ij} and Δ_i are similarly used.

The parameters used here are $P_1 = 30$ mW, $P_2 = 5$ mW, $P_3 = 15$ mW, $\Delta_1 = \Delta_3 = 2\pi \times 700$ MHz, $\Delta_2 = 2\pi \times 700$ MHz, $\Gamma_{20} = \Gamma_{30} = 2\pi \times 3$ MHz, $\Gamma_{00} = \Gamma_{10} = 0.01\Gamma_{20}$ and OD = 10. According to Eq. (14), we can predict the specific value of δ_i: $\delta_1 = 0$, Δ_1; $\delta_3 = -\Delta_2$, $\Delta_1/2 + \Omega_{e1}/2$, $\Delta_1/2 - \Omega_{e1}/2$. Due to satisfying the equation $\omega_1 + \omega_2 + \omega_3 = \varpi_{s1} + \delta_1 + \varpi_{s2} + \delta_2 + \varpi_{s3} + \delta_3(\delta_1 + \delta_2 + \delta_3 = 0)$, we can predict that the number of specific value of δ_2 is six, which indicates six types of SSWMs appearing in the interaction. Accordingly, we obtain Fig. 2, and correspondingly, six types of triphotons can be generated from these SSWM processes in the spontaneous emission. Every type of SSWM process should satisfy the conservation of energy. Fig. 2 shows six types of SSWMs. Similarly, we use this method to analyze $P_2(\delta_1, \delta_2)$ and $P_3(\delta_2, \delta_3)$. There are six types of SSWMs behind $P_2(\delta_1, \delta_2)$ and nine types of SSWMs behind $P_3(\delta_2, \delta_3)$.

The above analysis indicates that the fifth-order nonlinear susceptibilities $\chi^{(5)}$ control the parametric conversion efficiency of three input beams. The triphoton wave packet is determined by the nonlinearities and phase matchings. Correspondingly, the temporal coherence properties of the triplets are governed by both nonlinearities and phase criterion. In other words, we should focus on two regimes: the damped Rabi oscillation regime, which is determined by the nonlinear optical properties, and the group-delay regime, which is determined by the phase matchings. Comparing the triphoton spectral width governed by the nonlinear optical response with the width of the phase dispersion, the narrow one will play a major role in the triphoton wave packets.

The strong dressing field results in the coherence states in the "dressed-state" picture of the generated photons. The value of δ_i represents the resonance position of the "dressed-state" picture. Furthermore, the photon states of $\boldsymbol{E}_{S1}$, $\boldsymbol{E}_{S2}$ and $\boldsymbol{E}_{S3}$ that satisfy the energy conservation of $\delta_1 + \delta_2 + \delta_3 = 0$ can form one coherent channel of the SWM process. With the destructive interference among these coherent channels (Fig. 2), the triphoton coincidence counting rate is demonstrated as a coherent Rabi oscillation.

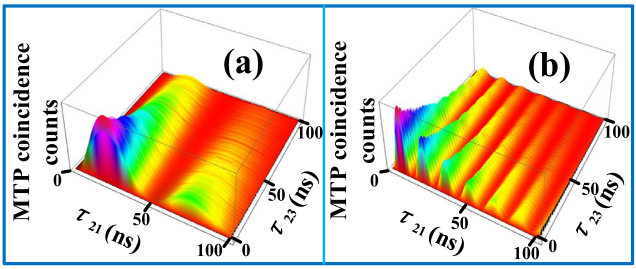

Fig. 3. Multimode triphoton coincidence counting rate in directions $\tau_{21} = t_1 - t_2$ and $\tau_{23} = t_3 - t_2$ of the damped Rabi oscillation regime. (a) $\Delta_1 = 120$ MHz; (b) $\Delta_1 = 400$ MHz.

5. Triphoton counting measurement

Section 3 indicates that the wave function of the triphoton is a convolution of nonlinear and linear optical responses, and the properties of the triphoton amplitude is determined by either response. Until now, we also know that the wave function results from the competition between linear and nonlinear optical responses. Here, we only discuss the nonlinear susceptibility. In this condition, the effective coupling Rabi frequency Ω_e make the multimode SWM channels occur, which can generate the multimode triphoton. With the multimode triphoton beating or destructive interference with each other, the wave function of the triphoton appears as a damped Rabi oscillation.

According to Sections 2 and 3, we obtain $\chi_{Si}^{(5)}$ and $\Phi = 1$. After some mathematical calculations, the triphoton coincidence counts can be written as

$$\begin{aligned} R_{c3} = |B_3|^2 = W_2[&e^{-2\Gamma_{10}\tau_{12}} + e^{-2\Gamma_{30}\tau_{12}} - 2e^{-(\Gamma_{10}+\Gamma_{30})\tau_{12}}\cos(\Delta_1\tau_{12})]e^{-2\Gamma_{e1}\tau_{23}}[\Omega_{e1}^2 e^{-2(\Gamma_{20}-\Gamma_{e1})\tau_{23}} \\ &+ \frac{\Omega_{e1}^2}{2}e^{-2\Gamma_{e1}\tau_{23}}(1-\cos(\Omega_{e1}\tau_{23})) \\ &- \Omega_{e1}(\Gamma_{20}-\Gamma_{e1})\sin(\Omega_{e1}\tau_{23}) + \Omega_{e1}(\Gamma_{20}-\Gamma_{e1})\sin(M_1\tau_{23}) - D_1\cos(M_1\tau_{23}) \\ &+ \Omega_{e1}(\Gamma_{20}-\Gamma_{e1})\sin(M_2\tau_{23}) - D_2\cos(M_2\tau_{23})], \end{aligned} \tag{17}$$

where $D_1 = \Omega_{e1}^2/2 + (\Delta_1/2 + \Delta_2)\, e^{-(\Gamma_{20}-\Gamma_{e1})\tau_{23}}$, $D_2 = \Omega_{e1}^2/2 - (\Delta_1/2 + \Delta_2)\, e^{-(\Gamma_{20}-\Gamma_{e1})\tau_{23}}$, $M_1 = \Omega_{e1}/2 + \Delta_1/2 + \Delta_2$, $M_2 = \Omega_{e1}/2 - \Delta_1/2 - \Delta_2$, $\tau_{12} = \tau_{S1} - \tau_{S2}$ and $\tau_{23} = \tau_{S2} - \tau_{S3}$. Obviously, the Rabi oscillation has one oscillation period that results from $2\pi/\Delta_1$ in direction τ_{12} and multiple oscillation periods that result from several sine functions in direction τ_{23}.

Here, we change the frequency of Δ_1 as shown in Fig. 3. With increasing frequency, the oscillation period in direction τ_{21} decreases. In addition, the counting rate decays with the effective dephasing rate, and the coherent time is determined by the effective dephasing rate. As shown in Fig. 3, we adopt two directions τ_{21} and τ_{23} to calculate the coincidence counts.

Next, we focus on the different method of coincidence counts. We use photon $\boldsymbol{E}s2$ as the trigger photon and other photons as the stop photons to complete the count ends from Eq. (17).

By changing the trigger photon and using different fifth-order susceptibilities and mathematical calculations, we obtain the triphoton coincidence counts with photons $\boldsymbol{E}s3$ and $\boldsymbol{E}s1$ as the trigger photons, respectively.

$$\begin{aligned} R_{c3} = |B_3|^2 = W_2[&e^{-2\Gamma_{10}\tau_{13}} + e^{-2\Gamma_{31}\tau_{13}} - 2e^{-(\Gamma_{10}+\Gamma_{31})\tau_{13}}\cos(\Delta_3\tau_{13})]e^{-2\Gamma_{e2}\tau_{23}}[\Omega_{e2}^2 e^{-2(\Gamma_{21}-\Gamma_{e2})\tau_{23}} \\ &+ \frac{\Omega_{e2}^2}{2}e^{-2\Gamma_{e2}\tau_{23}}(1-\cos(\Omega_{e2}\tau_{23})) - \Omega_{e2}(\Gamma_{21}-\Gamma_{e2})\sin(\Omega_{e2}\tau_{23}) \\ &+ \Omega_{e2}(\Gamma_{21}-\Gamma_{e2})\sin(\dot{M}_1\tau_{23}) - \dot{D}_1\cos(\dot{M}_1\tau_{23}) \\ &+ \Omega_{e2}(\Gamma_{21}-\Gamma_{e2})\sin(\dot{M}_2\tau_{23}) - \dot{D}_2\cos(\dot{M}_2\tau_{23})], \end{aligned} \tag{18}$$

where $\dot{D}_1 = \Omega_{e2}^2/2 + (\Delta_1/2 - \Delta_2)\, e^{-(\Gamma_{21}-\Gamma_{e2})\tau_{23}}$, $\dot{D}_2 = \Omega_{e2}^2/2 - (\Delta_1/2 - \Delta_2)\, e^{-(\Gamma_{21}-\Gamma_{e2})\tau_{23}}$, $\dot{M}_1 = \Omega_{e2}/2 + \Delta_1/2 - \Delta_2$, $\dot{M}_2 = \Omega_{e2}/2 - \Delta_1/2 + \Delta_2$.

$$
\begin{aligned}
R_{c3} = |B_3|^2 = W_2[&\frac{\Omega_{e3}^2}{2} e^{-2\Gamma_{e3}\tau_{12}} (1 - \cos(\Omega_{e3}\tau_{12})) - D\sin(\Omega_{e3}\tau_{12}) - \ddot{D}_2 \cos\left(\ddot{M}_2\tau_{12}\right) \\
&+ D\sin\left(\ddot{M}_1\tau_{12}\right) - \ddot{D}_1 \cos\left(\ddot{M}_1\tau_{12}\right) + D\sin\left(\ddot{M}_2\tau_{12}\right)] \\
e^{-2\Gamma_{e3}\tau_{12}} e^{-2\Gamma_{e4}\tau_{13}}[&\frac{\Omega_{e4}^2}{2} e^{-2\Gamma_{e4}\tau_{13}} (1 - \cos(\Omega_{e4}\tau_{13})) - D'\sin(\Omega_{e4}\tau_{13}) - \ddot{D}_4 \cos\left(\ddot{\ddot{M}}_2\tau_{13}\right) \\
&+ D'\sin(\ddot{\ddot{M}}_1\tau_{13}) - \ddot{D}_3 \cos(\ddot{\ddot{M}}_1\tau_{13}) + D'\sin(\ddot{\ddot{M}}_2\tau_{13})],
\end{aligned}
\tag{19}
$$

where D and D' are the constants. $\ddot{D}_1 = \Omega_{e3}^2/2 + (\Delta_1/2)\, e^{-(-\Gamma_{10}-\Gamma_{e3})\tau_{12}}$, $\ddot{D}_2 = \Omega_{e3}^2/2 - (\Delta_1/2)\, e^{-(-\Gamma_{10}-\Gamma_{e3})\tau_{12}}$, $\ddot{D}_3 = \Omega_{e4}^2/2 + (-\Delta_1/2 - \Delta_3)\, e^{-(\Gamma_{30}-\Gamma_{e4})\tau_{13}}$, $\ddot{D}_4 = \Omega_{e4}^2/2 - (-\Delta_1/2 - \Delta_3)\, e^{-(\Gamma_{30}-\Gamma_{e4})\tau_{13}}$, $\ddot{M}_1 = \Omega_{e3}/2 + \Delta_1/2$, $\ddot{M}_2 = \Omega_{e3}/2 - \Delta_1/2$, $\ddot{\ddot{M}}_1 = \Omega_{e4}/2 - \Delta_1/2 - \Delta_3$, and $\ddot{\ddot{M}}_2 = \Omega_{e4}/2 + \Delta_1/2 + \Delta_3$.

Fig. 4(a–c) show the theoretical curves of the triphoton coincidence counting rate in the damped Rabi oscillation regime by applying different trigger photons. When we employ $\boldsymbol{E}s3$ as the trigger photon, the Rabi oscillation only has one oscillation period in direction τ_{13}, while there are multiple oscillation periods in direction τ_{23}. In addition, when we use $\boldsymbol{E}s1$ as the trigger photon, there are multiple oscillation periods in dimensions τ_{12} and τ_{13}.

As shown in Fig. 4(a) and predicted from Eq. (17), there is only one oscillation period Δ_1 in direction τ_{12}. However, three oscillation periods Ω_{e1}, $\Omega_{e1}/2 + \Delta_1/2 + \Delta_2$ and $\Omega_{e1}/2 - \Delta_1/2 - \Delta_2$ exist in direction τ_{23}. These outcomes correspond with the fifth-order nonlinear susceptibility in Fig. 2. When we use $\boldsymbol{E}s2$ as the trigger photon, there are two modes in direction τ_{12}. Since there is destructive interference between the two modes, there is only one oscillation period, and the oscillation period is equal to the difference between the frequencies of the two modes ($\delta_1 = 0, \Delta_1$). There are also three modes in direction τ_{23}. Therefore, three oscillation periods in the direction τ_{23} are due to the destructive interference among the three modes, whereas the oscillation periods come from the difference in frequency of the three modes ($\delta_3 = \Delta_1/2 + \Omega_{e1}/2, \Delta_1/2 - \Omega_{e1}/2, -\Delta_2$). In fact, the number of oscillation periods in directions τ_{23} and τ_{12} is ten, respectively, which can be explained as follows. In Eq. (17), by replacing τ_{12} with $\tau_{13} - \tau_{23}$, the number of oscillation periods in direction τ_{23} becomes four. Similarly, we use $\tau_{13} - \tau_{12}$ to replace τ_{23}, and the oscillation periods in direction τ_{12} become four. The reason why there are three oscillation periods in the τ_{23} direction when using $\boldsymbol{E}s2$ as the trigger photon is that seven periods are hidden in this coordinate system. When we apply the same method to analyze Eqs. (18) and (19), there are four oscillation periods in Eq. (18) and six oscillation periods in Eq. (19).

Finally, we premeditate the situation of the mixture of the fifth-order nonlinear susceptibility and the phase matchings. As shown in Fig. 4(d), a sharp peak appears near the origin of the coordinates and is the precursor of the triphoton correlation. When the counting time is gradually away from the origin, the slow lights begin to regulate the wave packet of triphoton counting rates.

6. Conclusion

In conclusion, we discuss the optical responses of the generated fields in an atomic ensemble. The fifth-order nonlinear susceptibility $\chi_{S1}^{(5)}$ indicates the occurrence of six types of SSWMs in this process after the dressing field has been introduced. To further explore the properties of the generated photons, we calculate the triphoton coincidence counting rate using three different trigger photons. The nonlinear optical response plays a major role in determining the triphoton wave packet. The triphoton coincidence counting rate appears as a damped Rabi oscillation with the multimode triphoton beating caused by the destructive interference. These results can be of great significance to the fundamental tests of quantum mechanics and quantum information technologies.

Acknowledgments

This work was supported by the National Key R&D Program of China (2017YFA0303700, 2018YFA0307500), National Natural Science Foundation of China (61975159, 61605154, 11604256, 11804267, 11904279).

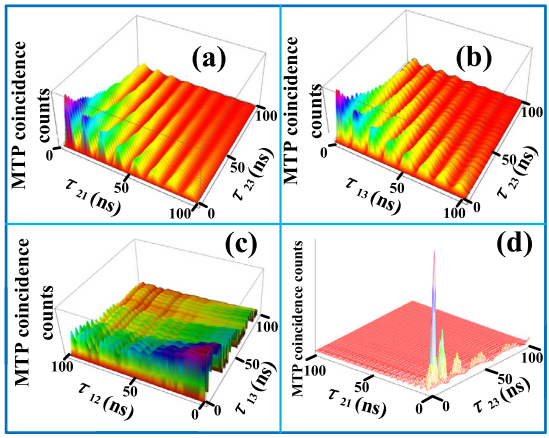

Fig. 4. (a) Multimode triphoton coincidence counting rate in directions $\tau_{21} = t_2 - t_1$ and $\tau_{23} = t_2 - t_3$ of the damped Rabi oscillation regime (using Eq. (17)). (b) Multimode triphoton coincidence counting rate in directions $\tau_{13} = t_1 - t_3$ and $\tau_{23} = t_2 - t_3$ of the damped Rabi oscillation regime (using Eq. (18)). (c) Multimode triphoton coincidence counting rate in directions $\tau_{12} = t_1 - t_2$ and $\tau_{13} = t_1 - t_3$ of the damped Rabi oscillation regime (using Eq. (19)). (d) Numerical simulation of the triphoton coincidence counting rate in Eq. (9).

References

[1] A. Steane, Rep. Prog. Phys. 61 (1997) 117.
[2] B. Zhao, Z.B. Chen, Y.A. Chen, J. Schmiedmayer, J.W. Pan, (2006).
[3] L.A. Lugiato, A. Gatti, E. Brambilla, A. Gatti, E. Brambilla, O. Jedrkiewicz, A. Maître, N. Treps, C. Fabre, N. Treps, J. Opt. B 4 (2002) 176.
[4] S.E. Harris, M.K. Oshman, R.L. Byer, Phys. Rev. Lett. 18 (1967) 732–734.
[5] H. Hübel, D.R. Hamel, A. Fedrizzi, S. Ramelow, K.J. Resch, T. Jennewein, Nature 466 (2010) 601–603.
[6] L.K. Shalm, D.R. Hamel, Z. Yan, C. Simon, K.J. Resch, T. Jennewein, Nat. Phys. 9 (2013) 19–22.
[7] P. Kolchin, S. Du, C. Belthangady, G.Y. Yin, S.E. Harris, Phys. Rev. Lett. 97 (2006) 113602.
[8] V. Balic, D.A. Braje, P. Kolchin, G.Y. Yin, S.E. Harris, Phys. Rev. Lett. 94 (2005) 183601.
[9] S.E. Harris, G.Y. Yin, A. Kasapi, M. Jain, Z.F. Luo, Phys. Today 50 (2006) 36–42.
[10] E. Oh, J. Wen, S. Du, J. Opt. Soc. Amer. B 27 (2010) A11–A20.
[11] J. Wen, S. Du, M.H. Rubin, Phys. Rev. A 75 (2007) 723–727.
[12] P. Kolchin, Phys. Rev. A 75 (2007) 723–727.
[13] J. Wen, M.H. Rubin, S. Du, J. Opt. Soc. Amer. B 25 (2008) C98–C108.
[14] J. Wen, S. Du, Y. Zhang, M. Xiao, M.H. Rubin, Phys. Rev. A 77 (2008) 156.
[15] C.I. Osorio, S. Barreiro, M.W. Mitchell, J.P. Torres, Phys. Rev. A 78 (2008) 4948–4954.
[16] J. Wen, S. Du, M.H. Rubin, Phys. Rev. A 76 (2007) 693–695.
[17] J. Wen, M.H. Rubin, Phys. Rev. A 74 (2006) 154.
[18] J. Wen, M.H. Rubin, Phys. Rev. A 74 (2006) 154, 154.
[19] C.H.R. Ooi, M.O. Scully, Phys. Rev. A 76 (2007) 538.
[20] S. Du, J. Wen, M.H. Rubin, G.Y. Yin, Phys. Rev. Lett. 98 (2007) 53601.
[21] V. Balic, D.A. Braje, P. Kolchin, G.Y. Yin, S.E. Harris, Phys. Rev. Lett. 94 (2005) 183601.
[22] S. Du, P. Kolchin, C. Belthangady, G.Y. Yin, S.E. Harris, Phys. Rev. Lett. 100 (2008) 183603.
[23] B.S. Shi, D.S. Ding, G.C. Guo, S. Shi, W. Zhang, Y. Li, Z.Y. Zhou, Optica 2 (2015) 642.
[24] Z. Nie, H. Zheng, P. Li, Y. Yang, Y. Zhang, M. Xiao, Phys. Rev. A 77 (2008) 3195–3199.